Bull. Mater. Sci., Vol. 38, No. 2, April 2015, pp. 365–372. © Indian Academy of Sciences.

First-principle calculations of the structural, electronic, thermodynamic and thermal properties of ZnS_xSe_{1-x} ternary alloys

S BENDAIF[1], A BOUMAZA[1], O NEMIRI[1], K BOUBENDIRA[1], H MERADJI[1,*], S GHEMID[1] and F EL HAJ HASSAN[2]

[1]Laboratoire LPR, Département de Physique, Faculté des Sciences, Université Badji Mokhtar, Annaba 23000, Algeria
[2]Laboratoire de Physique et d'électronique, Faculté des Sciences, Université Libanaise, Elhadath, Beirut 6573-14, Lebanon

MS received 20 November 2013; revised 12 May 2014

Abstract. **First-principle calculations were performed to study the structural, electronic, thermodynamic and thermal properties of ZnS_xSe_{1-x} ternary alloys using the full potential-linearized augmented plane wave method (FP-LAPW) within the density functional theory (DFT). In this approach the Wu–Cohen generalized gradient approximation (WC-GGA) and Perdew–Wang local density approximation (LDA) were used for the exchange–correlation potential. For band structure calculations, in addition to WC-GGA approximation, both Engel–Vosko (EV-GGA) generalized gradient approximation and recently proposed modified Becke–Johnson (mBJ) potential approximation have been used. Our investigation on the effect of composition on lattice constant, bulk modulus and band gap for ternary alloys shows a linear dependence on alloy composition with a small deviation. The microscopic origins of the gap bowing were explained using the approach of Zunger and co-workers. Besides, a regular-solution model was used to investigate the thermodynamic stability of the alloys which mainly indicates a phase miscibility gap. Finally, the quasi-harmonic Debye model was applied to see how the thermal properties vary with temperature at different pressures.**

Keywords. **FP-LAPW; DFT; energy band structure; thermal properties; Debye model; critical temperature.**

1. Introduction

Zinc-based semiconductor compounds have attracted considerable theoretical and experimental interest in the last decades since they have a potential to be employed as base materials for light-emitting and laser diodes, infrared detectors, photovoltaic devices and quantum dots applications.[1] ZnS and ZnSe semiconductor compounds have attracted significant interest for their potential applications in opto-electronics and electronics.[2–5] ZnS and ZnSe crystallize in the zinc-blende structure and are characterized by a large and direct gap of 3.68 eV for ZnS[6] and 2.69 eV for ZnSe.[6] Therefore, the application of band gap engineering to ZnSSe ternary alloys, which can be obtained as a result of the band gap engineering of ZnSe and ZnS, would be of great interest to researchers aiming to develop optoelectronic or photonic devices with high performance. Several studies have examined the tunability of the energy band gap of ZnSe by adding sulphur as an alloying element to ZnSe.[7–10] The ternary alloy ZnS_xSe_{1-x}, has been extensively used for designing opto-electronic devices.[11–15] Although a number of experimental[9,16–20] and theoretical studies[6,21–26] of ZnS_xSe_{1-x} semiconductor alloys have been published, to the best of our knowledge there are no available data for their thermal properties. Usually, the thermodynamic properties of materials are the basis of solid-state science and industrial applications. Furthermore, thermodynamic properties for crystalline materials are very important in many applications involving high pressure and high temperature. Although *ab-initio* calculations have successively predicted the electronic and structural properties of various materials, these calculations are very often restricted to the 0 K temperatures. In this work, thermal properties are considered by the use of the quasi-harmonic Debye model,[27] and in order to provide another reference data for completing the existing theoretical and experimental works on these alloys, we have performed the present work using the full-potential augmented plane-wave method (FP-LAPW) based on the density functional theory (DFT) combined with the quasi-harmonic Debye model. The paper is organized as follows: computational details are described in section 2. The obtained results are presented in section 3. Finally, we present the main conclusions of the present work in section 4.

2. Method of calculations

The calculations presented in this work were performed using the FP-LAPW method[28] within the framework of the

*Author for correspondence (hmeradji@yahoo.fr)

DFT[29,30] as implemented in the Wien2k code[31] that has been shown to yield reliable results for the electronic and structural properties of various solids. For structural properties, the exchange–correlation potential was calculated using the Perdew–Burke–Ernzerhof generalized gradient approximation (PBE-GGA),[32] Wu–Cohen generalized gradient approximation (WC-GGA)[33] which is an improved form of the most popular (PBE-GGA) and Perdew–Wang local density approximation (LDA).[34] In addition, and for electronic properties, we used the Engel and Vosko GGA (EV-GGA),[35] and the modified Becke–Johnson (mBJ)[36,37] schemes, this later was designed to reproduce as well as possible the exact exchange-correlation potential rather than the total energy, and as a result gives significantly improved results such as band gap and electronic structure. This gives us a unique opportunity to test the accuracies of the potentials employed and the calculation schemes in general. In the FP-LAPW method, primitive unit cell is divided into two regions (non-overlapping muffin tin spheres surrounding the atomic sites and an interstitial region). Inside the muffin-tin spheres, the wave electron charge densities and potentials were expanded in terms of the spherical harmonics, while for the interstitial region between the spheres, plane wave expansions were used. The maximum l value for the wave function expansions inside spheres was confined to $l_{\max} = 10$. The plane wave cut-off of $K_{\max} = 8.0/R_{\mathrm{MT}}$ is chosen for the expansion of the wave functions in the interstitial region, while the charge density was Fourier expanded up to $G_{\max} = 14$ (Ryd)$^{1/2}$. The muffin-tin radius R_{MT} were assumed to be 2.24, 1.98 and 1.98 for Zn, S and Se atoms, respectively. A mesh of 47 special k-points for binary compounds and 125 special k-points for alloys were taken in the irreducible wedge of the Brillouin zone for the total energy calculation. Both the plane wave cut-off and the number of k-points are varied to ensure total energy convergence.

3. Results and discussion

3.1 *Structural properties*

Firstly, we calculated the structural properties of the binary compounds ZnS, ZnSe and their ternary alloys in the zinc-blende phase using the PBE-GGA and WC-GGA schemes. The alloys are modelled at some selected compositions with ordered structures described in terms of periodically repeated supercells. For the compositions $x = 0.25$, 0.50 and 0.75, the simplest structure is an eight-atom simple cubic lattice. For the compositions $x = 0.25$ and 0.75 the simplest structure is an eight-atom simple cubic cell (luzonite): the anions with the lower concentration form a regular simple cubic lattice. For the composition $x = 0.5$, the atoms of the same layer are identical. The idea of constructing an alloy by taking a large unit cell (cubic eight atoms) and repeating it three dimensionally for the calculation of the electronic structure of alloys has been used by Agrawal *et al*.[38] In recent times, many researchers have used this method to investigate properties of alloys.[39–41] For the structures considered, we performed the structural optimization by minimizing the total energy with respect to the cell parameters and also the atomic positions. The total energies calculated as a function of unit cell volume are fitted to the Murnaghan equation of state[42] to determine the ground state properties such as the equilibrium lattice constant a, the bulk modulus B and its pressure derivative B'. Our results concerning the lattice constant and the bulk modulus are collected in table 1. Also shown for comparison are the available experimental and theoretical data reported in the literature. The present WC-GGA results agree well with the previous experimental reports for the binary compounds, hence, it is reasonable to expect that the lattice constant and bulk modulus of the alloys can be described with similar accuracy in our calculations. In view of table 1, it is clear that the calculated bulk modulus value decreases from

Table 1. Calculated lattice parameter a (Å) and bulk modulus B (GPa) for the binary compounds ZnS and ZnSe and their alloys ZnS_xSe_{1-x} at equilibrium volume.

	Lattice constant a (Å)					Bulk modulus B (GPa)				
	This work					This work				
	WC-GGA	PBE-GGA	LDA	Exp	Other calculations	WC-GGA	PBE-GGA	LDA	Exp	Other calculations
0	5.658	5.753	5.590		5.669[a], 5.746[b] 5.57[c], 5.68[d], 5.71[e]	66.335	57.308	70.429	62.5[a]	57.046[b], 69.6[c] 66.2[d], 62.9[e]
0.25	5.592	5.684	5.534			68.855	60.086	72.411		
0.5	5.524	5.613	5.469			72.718	63.172	73.332		
0.75	5.451	5.538	5.404			76.033	66.006	86.715	—	
1	5.376	5.460	5.376	5.411[a]	5.46[b], 5.30[c] 5.42[d], 5.47[e]	79.953	70.006	87.970	76.9[a]	73.761[b], 81.2[c] 81.8[d], 82.6[e]

[a]Ref 53, [b]Ref 26, [c]Ref 25, [d]Ref 54, [e]Ref 46.

ZnS to ZnSe, suggesting that the compressibility increases from ZnS to ZnSe. Henceforth, the lattice parameter enlargement and the reduction in bulk modulus indicate the softening tendency of lattice on increasing size of chalcogens. We note that the zinc atom is the same in the two compounds, so the chalcogen S and Se atoms size could be the responsible for the lattice constant increasing from ZnS to ZnSe.

The composition dependence of the calculated lattice constant for ZnS_xSe_{1-x} alloys is shown in figure 1. We can note that, as the composition x increases the lattice constant decreases monotonically and almost linearly exhibiting an upward weak bowing parameter equal to -0.0457 Å obtained by fitting the calculated values with a polynomial function. This is consistent with Vegard's law which assumes that the lattice constant varies linearly with the alloy composition[43] (figure 1, dashed line). There is a good agreement between our results and the previously reported experimental findings[44,45] and theoretical data.[25,45,46] The substitution of the Se atom by the S atom decreases the lattice constant, which is probably due to smaller atom radius of S than that of Se.

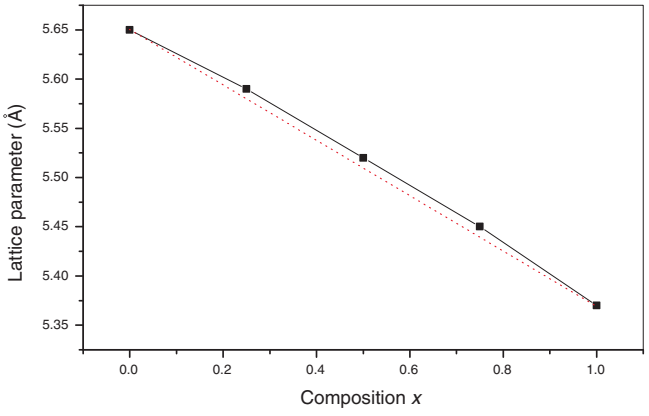

Figure 1. Composition dependence of the calculated lattice constants (solid squares) of ZnS_xSe_{1-x} alloys compared with Vegard's prediction (dashed line) using WC-GGA approximation.

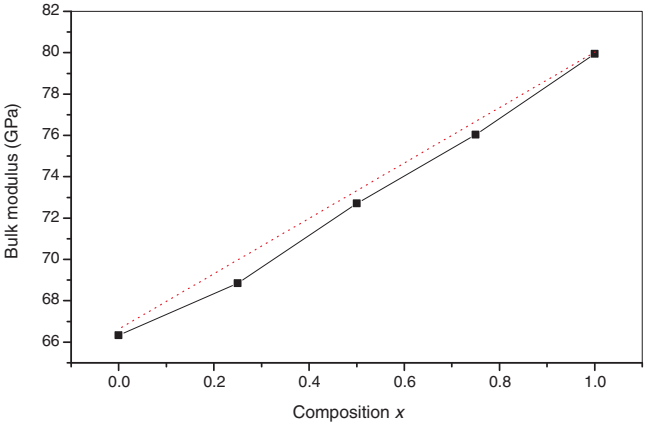

Figure 2. Composition dependence of the calculated bulk modulus (solid squares) of ZnS_xSe_{1-x} alloys compared with the linear composition dependence prediction (dashed line) using WC-GGA approximation.

The composition dependence of the bulk modulus for the alloys under investigation is compared with the results predicted by linear concentration dependence (LCD) in figure 2. A small deviation from LCD, with downward bowing equal to 2.582 GPa was observed. This deviation is mainly due to the mismatch of the bulk modulus of the binary compounds ZnS and ZnSe. It is clearly seen that the bulk modulus increases with the decrease in the chalcogenide atomic number. Hence, we conclude that ZnSe is more compressible than ZnS.

3.2 *Electronic properties*

The calculated band structure energies of binary compounds, as well as for their alloys using PBE-GGA, EV-GGA and mBJ schemes indicate a direct band gap at the Γ point in the whole range of concentrations. The results are given in table 2, and compared with the theoretical values and the available experimental data. It is found that for the PBE-GGA, the energy gap is underestimated compared to the experimental value which is due to the well-known trend of the generalized

Table 2. Direct band gap energy (Γ–Γ) of ZnS_xSe_{1-x} alloys at different *S* concentrations (all values are in eV).

	E_g (eV) Γ–Γ				
	This work				
x	WC-GGA	EV-GGA	mBJ	Exp.	Other calculations
0	1.12	2.09	2.75	2.69[a]	2.67[b], 1.31[d], 2.24[e]
0.25	1.32	2.31	2.98		
0. 5	1.71	2.53	3.23		
0.75	1.76	2.79	3.46		
1	1.99	3.05	3.72	3.68[a]	3.66[b], 1.969[c], 2.16[d], 3.38[e]

[a]Ref 6, [b]Ref 55(mBJ), [c]Ref 56 (PBE-GGA), [d]Ref 57 (LDA), [e]Ref 58 (GW).

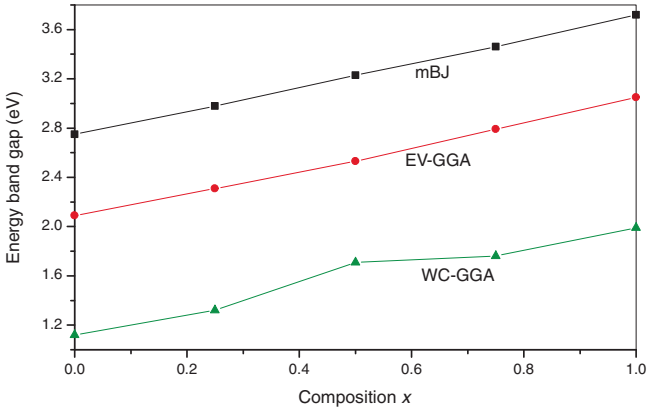

Figure 3. Composition dependence of the calculated band gap using mBJ, EV-GGA and WC approximations for ZnS_xSe_{1-x} alloys.

gradient approximation, while EV-GGA scheme gives quite a nice band gap compared to the experimental one, the mBJ gives significantly improved results (see table 2) which are very close to the experimental values. According to current calculations, mBJ performed better than other conventional DFT functionals to calculate band structure. It can be used to model the electronic properties of semiconductors. The calculated band gap *vs.* concentration was fitted by a polynomial equation. The results are shown in figure 3 and are summarized as follows:

$$\mathrm{ZnS}_x\mathrm{Se}_{1-x} \Rightarrow \begin{cases} E_g^{\mathrm{mBJ}} = 2.751 + 0.876x + 0.091x^2, \\ E_g^{\mathrm{EV\text{-}GGA}} = 2.091 + 0.822x + 0.137x^2, \\ E_g^{\mathrm{WC\text{-}GGA}} = 1.104 + 1.192x - 0.320x^2. \end{cases} \quad (1)$$

In order to better understand the physical origins of the band-gap bowing in these alloys, we have followed the procedure of Bernard and Zunger,[47] in which the bowing parameter (b) is decomposed into three physically distinct contributions. In fact the overall band gap bowing coefficient at $x = 0.50$ measures the change in the band gap according to the reaction:

$$\mathrm{ZnS}(a_{\mathrm{ZnS}}) + \mathrm{ZnSe}(a_{\mathrm{ZnSe}}) \rightarrow \mathrm{ZnS}_{0.5}\mathrm{Se}_{0.5}(a_{\mathrm{eq}}), \quad (2)$$

where a_{ZnS} and a_{ZnSe} are the equilibrium lattice constants of the binary compounds ZnS and ZnSe, respectively, and a_{eq} is the alloy equilibrium lattice constant. We now decompose reaction (2) into three steps:

$$\mathrm{ZnS}(a_{\mathrm{ZnS}}) + \mathrm{ZnSe}(a_{\mathrm{ZnSe}}) \xrightarrow{\mathrm{VD}} \mathrm{ZnS}\,(a) + \mathrm{ZnSe}(a), \quad (3)$$

$$\mathrm{ZnS}(a) + \mathrm{ZnSe}(a) \xrightarrow{\mathrm{CE}} \mathrm{ZnS}_{0.5}\mathrm{Se}_{0.5}(a), \quad (4)$$

$$\mathrm{ZnS}_{0.5}\mathrm{Se}_{0.5}(a) \xrightarrow{\mathrm{SR}} \mathrm{ZnS}_{0.5}\mathrm{Se}_{0.5}(a_{\mathrm{eq}}). \quad (5)$$

The first step measures the volume deformation (VD) effect on the bowing parameter. The corresponding contribution to the total band-gap bowing parameter b_{VD} represents the relative response of the band structure of the binary compounds ZnS and ZnSe to hydrostatic pressure, which here arises from the change of their individual equilibrium lattice constants to the alloy value $a = a\,(x)$ (Vegard's rule). The second contribution, the charge-exchange (CE) contribution b_{CE}, reflects a charge-transfer effect which is due to the different (averaged) bonding behaviours at the lattice constant a. The final step measures changes due to the structural relaxation (SR) in passing from the unrelaxed to the relaxed alloy by b_{SR}. Consequently, the total gap bowing parameter is defined as

$$b = b_{\mathrm{VD}} + b_{\mathrm{CE}} + b_{\mathrm{SR}}, \quad (6)$$

$$b_{\mathrm{VD}} = 2\left[E_g^{\mathrm{ZnS}}(a_{\mathrm{ZnS}}) - E_g^{\mathrm{ZnS}}(a) + E_g^{\mathrm{ZnSe}}(a_{\mathrm{ZnSe}}) - E_g^{\mathrm{ZnSe}}(a)\right], \quad (7)$$

$$b_{\mathrm{CE}} = 2\left[E_g^{\mathrm{ZnS}}(a) + E_g^{\mathrm{ZnSe}}(a) - 2E_g^{\mathrm{ZnSSe}}(a)\right], \quad (8)$$

$$b_{\mathrm{SR}} = 4\left[E_g^{\mathrm{ZnSSe}}(a) - E_g^{\mathrm{ZnSSe}}(a_{\mathrm{eq}})\right], \quad (9)$$

where E_g is the energy band gap, calculated for the indicated compound with the indicated atomic structures and lattice constants. We calculated the bowing contributions at composition $x = 0.5$ on the basis of equations (7–9) and the results are given in table 3, together with the bowing obtained using a quadratic variation of the band gap energy *vs.* composition x.

It can be seen that the calculated quadratic parameters (gap bowing) within mBJ and EV-GGA are very close to their corresponding results obtained by the Zunger approach. The low value of the bowing parameter is attributed to the weak mismatch of the lattice constants of ZnS and ZnSe compounds and the weak electronegativity difference between S (2.58) and Se (2.55) atoms.

3.3 *Thermodynamic properties*

We investigate here the phase stability of ternary alloy solid solution systems based on the regular-solution model.[48] At finite temperature, the thermal stability of a solid-state system is determined by the Gibbs free energy given by the following expression:[49]

$$\Delta G_{\mathrm{m}} = \Delta H_{\mathrm{m}} - T\Delta S_{\mathrm{m}}, \quad (10)$$

where

$$\Delta H_{\mathrm{m}} = \Omega x(1-x) = E_{\mathrm{Tot}}^{\mathrm{A}_x B_{1-x} C} - xE_{\mathrm{Tot}}^{\mathrm{AC}} - (1-x)E_{\mathrm{Tot}}^{\mathrm{BC}}, \quad (11)$$

$$\Delta S_{\mathrm{m}} = R\left[x\,\ln x + (1-x)\ln(1-x)\right], \quad (12)$$

Table 3. Decomposition of bowing parameter into volume deformation b_{VD}, charge exchange b_{CE} and structural relaxation b_{SR} contributions compared with the bowing parameter obtained by quadratic interpolation (all values are in eV).

		Zunger approach			Quadratic fits		
Alloy		mBJ	EV-GGA	WC-GGA	mBJ	V-GGA	WC-GGA
$\mathrm{ZnS}_x\mathrm{Se}_{1-x}$	b_{VD}	−0.001	0.048	0.064			
	b_{CE}	0.054	0.013	0.011			
	b_{SR}	0.050	0.073	0.659			
	b	0.102	0.134	0.606	0.091	0.137	0.32

ΔH_m and ΔS_m are the enthalpy and the entropy of mixing, respectively; Ω the interaction parameter which depends on the material; R the gas constant and T the absolute temperature. We then calculated ΔH_m to obtain Ω as a function of concentration. The interaction parameter increases almost linearly with increasing x. From a linear fit we obtained: Ω (kcal mol^{-1}) = 1.252x+2.681. The average value of the x-dependent Ω in the range $0 \leq x \leq 1$ obtained from this equation for ZnS_xSe_{1-x} alloys is 3.307 kcal mol^{-1}. We can calculate accurately the free energy of mixing ΔG_m using equations (11 and 12), then we use ΔG_m at different concentrations to calculate the $T-x$ phase diagram, which shows the stable, metastable and unstable mixing regions of the alloy. At a temperature lower than the critical temperature T_c, the two binodal points are determined as those points at which the common tangent line touches the ΔG_m curves, whereas the two spinodal points are determined as those points at which the second derivative of ΔG_m is zero; $\delta^2(\Delta G_m)/\delta x^2 = 0$. Figure 4 displays the calculated phase diagrams including the spinodal and binodal curves of the alloy of interest. We found a critical temperature T_c of 831.49 K. The spinodal curve in the phase diagram marks the equilibrium solubility limit, i.e., the miscibility gap. For temperatures and compositions above this curve a homogeneous alloy is predicted. The wide range between spinodal and binodal curves indicates that the alloy may exist as a metastable phase. Hence our results indicate that the alloy ZnS_xSe_{1-x} is stable at high temperature.

3.4 *Thermal properties*

To investigate the thermal properties of ZnS_xSe_{1-x} alloys, the quasi-harmonic Debye model[27] was applied, in which the non-equilibrium Gibbs function $G^*(V; P, T)$ can be written in the form of

$$G^*(V; P, T) = E(V) + PV + A_{vib}[\theta(V); T], \quad (13)$$

where $E(V)$ is the total energy per unit cell, PV corresponds to the constant hydrostatic pressure condition, $\theta(V)$ is the Debye temperature, and A_{vib} is the vibrational term, which can be written using the Debye model of the phonon density of state as[50,51]

$$A_{vib}(\theta; T) = nk_BT\left[\frac{9\theta}{8T} + 3\ln\left(1 - e^{-\theta T}\right) - D\left(\frac{\theta}{T}\right)\right], \quad (14)$$

where n is the number of atoms per formula unit $D(\theta/T)$ represents the Debye integral and for an isotropic solid, θ is expressed as[50]

$$\theta_D = \frac{\hbar}{k_B}\left[6\pi^2V^{1/2}n\right]^{1/3} f(\sigma)\sqrt{\frac{B_s}{M}}, \quad (15)$$

M being the molecular mass per unit cell and B_s the adiabatic bulk modulus, approximated by the static compressibility[27]

$$B_s \cong B(V) = V\left\{\frac{d^2E(V)}{dV^2}\right\}. \quad (16)$$

$f(\sigma)$ is given by

$$f(\sigma) = \left\{3\left[2\left(\frac{21+\sigma}{31-2\sigma}\right)^{3/2} + \left(\frac{11+\sigma}{31-\sigma}\right)^{3/2}\right]^{-1}\right\}^{1/3}. \quad (17)$$

The Poisson ratio σ is taken as 0.25.[52] Therefore, the non-equilibrium Gibbs function $G^*(V; P, T)$ as a function of $(V; P, T)$ can be minimized with respect to volume V

$$\left[\frac{\partial G^*(V; P, T)}{\partial V}\right]_{P,T} = 0. \quad (18)$$

By solving equation (18), one can get the thermal equation of state (EOS), $V(P, T)$. The isothermal bulk modulus B_T, the heat capacity C_v and the thermal expansion coefficient α are given by[27]

$$B_T(P, T) = V\left(\frac{\delta^2G^*(V; P, T)}{\delta V^2}\right)_{P,T}, \quad (19)$$

$$C_v = 3nk_B\left[4D\left(\frac{\theta}{T}\right) - \frac{3\theta/T}{e^{\theta/T} - 1}\right], \quad (20)$$

$$S = nk\left[4D\left(\frac{\theta}{T}\right) - 3\ln\left(1 - e^{-\theta T}\right)\right], \quad (21)$$

$$\alpha = \frac{\gamma C_V}{B_T V}, \quad (22)$$

where γ is the Grüneisen parameter, which is defined as

$$\gamma = -\frac{d\ln\theta(V)}{d\ln V}. \quad (23)$$

As a first step, a set of total energy calculation *vs.* primitive cell volume ($E - V$), in the static approximation, was carried

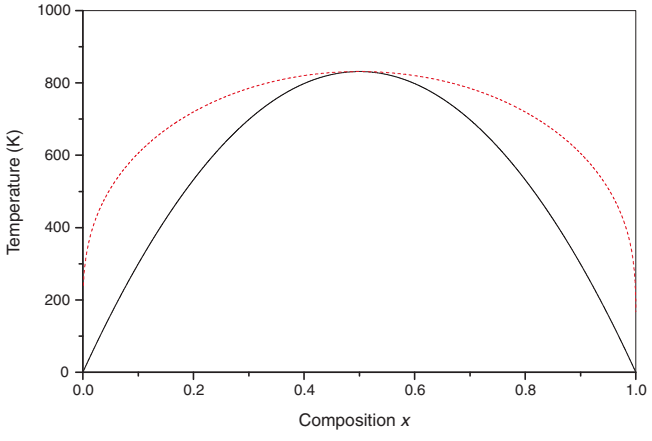

Figure 4. $T-x$ phase diagram of ZnS_xSe_{1-x} alloys.

out and fitted with a numerical equation of state in order to determine its structural parameters at $P = 0$ and $T = 0$, and then derive the macroscopic properties as function of P and T from standard thermodynamic relations. The thermal properties are determined in the temperature range from 0 to 900 K, where the quasi-harmonic model remains fully valid. The pressure effect is studied in the 0–6 GPa range. It is worthy to note that the previous theoretical calculations gave material properties at zero temperature only, without any thermal effects included, so the present work is the first theoretical prediction for these thermal quantities. Since the obtained results show a similar behaviour for the all concentrations, we have only presented the results related to the concentration 0.5.

In figure 5, we present the lattice constant-temperature diagram of $ZnS_{0.5}Se_{0.5}$ alloy at several pressures. The lattice constant increases with the increase in the temperature at a given pressure. On the other side, as the pressure increases, the lattice constant decreases at a given temperature. The rate of increase of the lattice constant with temperature decreases with the increase in the pressure. Temperature can cause cell expansion and pressure can suppress this effect. Figure 6 shows the evolution of the bulk modulus B of $ZnS_{0.5}Se_{0.5}$ alloy with temperature T at different pressures. The bulk modulus is nearly constant from 0 to 100 K and decreases almost linearly with increasing temperature for $T > 100$ K. The compressibility increases with increasing temperature at a given pressure and decreases with pressure at a given temperature. The hardness of this material decreases with the increase in the temperature and increases with applied pressure.

Figure 7 displays the dependence of the Debye temperature θ_D on temperature and pressure. It can be seen that θ_D is nearly constant from 0 to 100 K and decreases linearly with the increase in the temperature from $T > 100$ K. It is also shown that θ_D increases with applied pressure at a given temperature. We can see that the Debye temperature has a similar behavior with the bulk modulus regarding its variation with temperature and pressure. This result is in accordance with the fact that Debye temperature is proportional to the bulk modulus and that a hard material exhibits a high Debye temperature.

The knowledge of the heat capacity of a substance not only provides essential insight into its vibrational properties but is also mandatory for many applications. The obtained constant volume heat capacity C_v of $ZnS_{0.5}Se_{0.5}$ at various pressures and temperatures is plotted in figure 8. It is shown that when $T < 500$ K, the heat capacity C_v is depending on both temperature and pressure. This is due to the anharmonic approximations of the Debye model used in our calculations. However, at higher temperature, the anharmonic effect on C_v is suppressed, and C_v is very close to the Dulong–Petit limit, which is followed to all solids at high temperature. At high temperatures C_v approaches approximately 49.57 J $mol^{-1}K^{-1}$ for the alloy under investigation. On the other side, the details of this change depend on the pressure. The initial increase in C_v with temperature under low pressure is more rapid than under higher pressure. The variation of the heat capacity at constant pressure C_p *vs.* temperature at various pressures is depicted in figure 9. The variations of C_p for the studied alloy exhibit similar features.

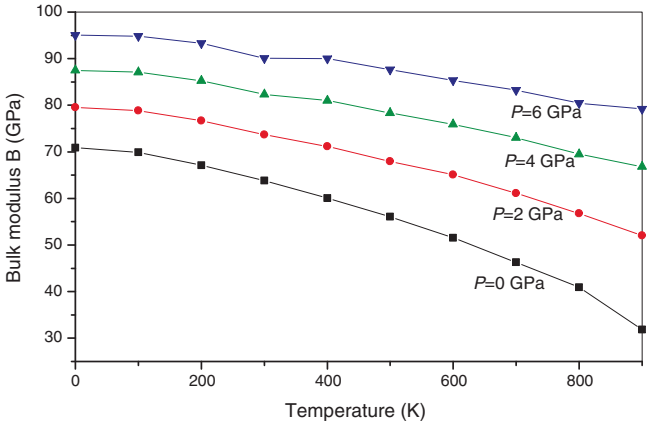

Figure 6. Variation of the bulk modulus with temperature at different pressures for $ZnS_{0.5}Se_{0.5}$ alloy.

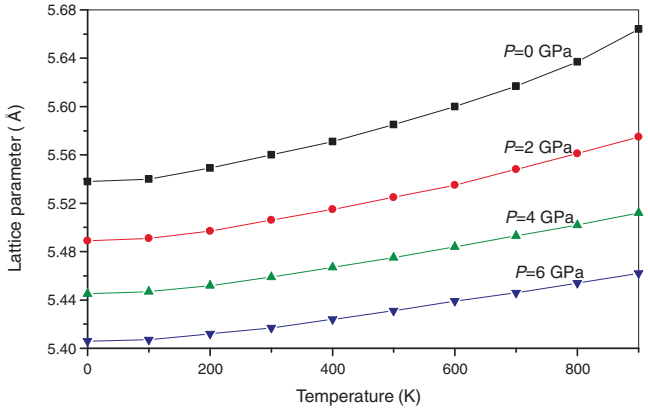

Figure 5. Relationship between lattice parameter and temperature at different pressures for $ZnS_{0.5}Se_{0.5}$ alloy.

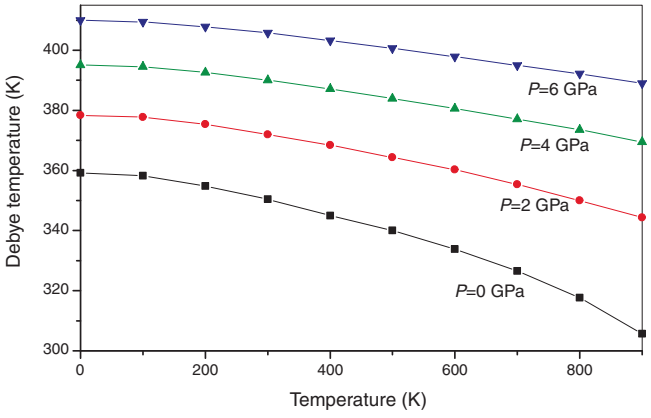

Figure 7. Debye temperature as a function of temperature at different pressures for $ZnS_{0.5}Se_{0.5}$ alloy.

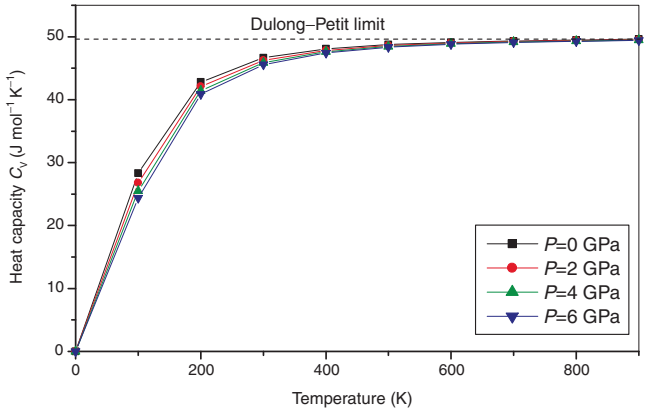

Figure 8. Variation of the heat capacity C_v with temperature at different pressures for $ZnS_{0.5}Se_{0.5}$ alloy.

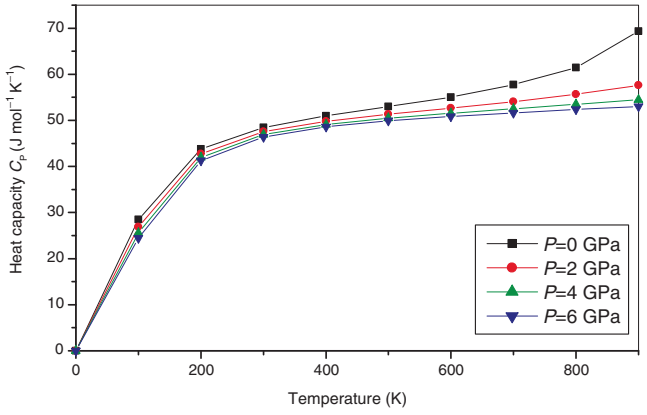

Figure 9. Variation of the heat capacity C_p with temperature at different pressures for $ZnS_{0.5}Se_{0.5}$ alloy.

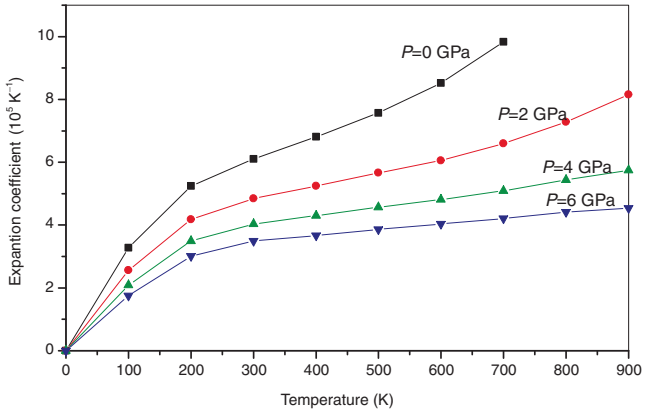

Figure 10. Variation of the volume expansion coefficient α as a function of temperature at different pressures for $ZnS_{0.5}Se_{0.5}$ alloy.

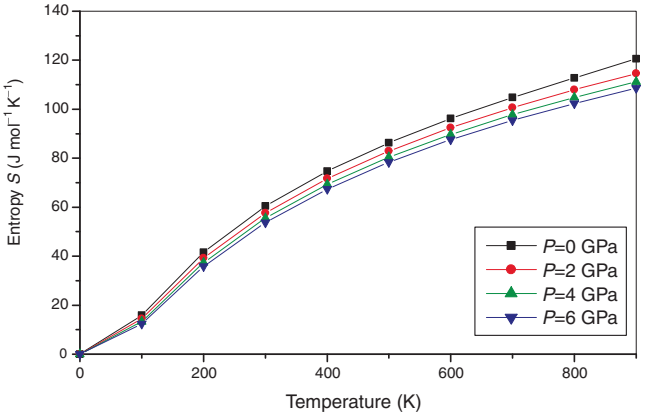

Figure 11. Variation of the entropy S with temperature at different pressures for $ZnS_{0.5}Se_{0.5}$ alloy.

With increasing temperature, variation features of C_p values at lower temperature are similar to that of C_v. However, in the high-temperature range, the change tendency of C_p exhibits apparently different features under different pressures. C_p values decrease with increasing pressures and do not converge to a constant value. In particular, at zero pressure, the heat capacity C_p increases rapidly at higher temperature.

Figure 10 shows the variation of the thermal expansion coefficient α with respect to the temperature at several pressures. The thermal expansion coefficient increases as the temperature increases. At zero pressure, the increase is the most drastic. For a given temperature, α decreases drastically with the increase of pressure. With increasing pressure, the increase in α is weakened. When $T > 300$ K, α gradually approaches a linear increase with enhanced temperature and the propensity of increment becomes moderate, which means that the temperature dependence of α is very small at high temperature.

The dispersal of energy and matter is described by the entropy, denoted by the symbol S. On a microscopic scale, the entropy can be defined as a measure of disorder of a system. The pressure and temperature dependence of the entropy S of $ZnS_{0.5}Se_{0.5}$ is plotted in figure 11. As the temperature increases, the vibrational contribution to the entropy increases and therefore the entropy increases with temperature. It is well known that, as the temperature rises, the contribution of phonons becomes more important.

4. Conclusions

Employing the FP-LAPW method based on the DFT within the generalized gradient approximation and the modified Becke–Johnson approximation, we have studied the structural, electronic, thermodynamic and thermal properties of ZnS_xSe_{1-x}.

A summary of our results follows:

(1) The estimated structural properties, as lattice constants and bulk modulus agree well with the experimental and the theoretical values. The calculated lattice parameters for the alloys exhibit a tendency to Vegard's law with a marginal bowing parameter.

(2) The use of the Modified Becke–Johnson scheme improves significantly the band gap which becomes closer to the experimental one. An almost linear

variation of band gap *vs.* concentration x has been observed leading to a small value of the bowing parameter.

(3) The calculated phase diagram indicated that ZnS_xSe_{1-x} is stable at temperature of 831.49 K.

(4) Finally, the quasi-harmonic Debye model is successfully applied to determine the thermal properties at different temperatures and pressures. The results presented in this paper for the thermodynamic and thermal properties are predictions, and the experiments to prove them are welcomed.

References

1. Boutaiba F *et al* 2009 *Superlattices Microstruct.* **46** 823
2. Prevenslik T V 2000 *J. Lumin.* **87** 1210
3. Yamamoto T *et al* 2001 *Physica B* **308** 916
4. Zhu Y and Bando Y 2003 *Chem. Phys. Lett.* **377** 367
5. Mirov S B 2002 *Opt. Lett.* **27** 909
6. Janetzko F and Jug K 2004 *J. Phys. Chem. A* **108** 5449
7. Xu H *et al* 2008 *Adv. Mater.* **20** 3294
8. Wang M *et al* 2007 *Adv. Mater.* **19** 4491
9. El-Shazly A A *et al* 1985 *Appl. Phys. A* **36** 51
10. Kumar V and Sharma T P 1998 *Opt. Mater.* **10** 253
11. Kim J S *et al* 1996 *Solid State Commun.* **100** 817
12. Wu B J *et al* 1996 *Appl. Phys. Lett.* **68** 379
13. Han J *et al* 1997 Eds *II–VI blue/green light emitters: device physics and epitaxial growth, semiconductor and semimetals* **44** 17
14. Godlewski M *et al* 2003 *J. Lumin.* **102** 455
15. Shen D *et al* 2003 *J. Mater. Sci. Lett.* **22** 483
16. Okuyama H *et al* 1998 *Phys. Rev. B* **57** 2257
17. Borna H *et al* 1998 *J. Cryst. Growth* **184/185** 1132
18. Song J H *et al* 2000 *J. Cryst. Growth* **214/215** 460
19. Sunghoon Park *et al* 2012 *Curr. Appl. Phys.* **12** 499
20. Tang T P *et al* 2009 *J. Alloys Compd.* **488** 250
21. Bernard J E and Zunger A 1987 *Phys. Rev. B* **36** 3199
22. Gabrel'yan B V *et al* 2000 *J. Struct. Chem.* **41** 403
23. Kassali K and Bouarissa N 2002 *Mater. Chem. Phys.* **76** 255
24. Benkabou F *et al* 2003 *Physica B* **337** 147
25. Mesri D *et al* 2007 *Comput. Mater. Sci.* **39** 453
26. Hakan Gürel H *et al* 2013 *Mater. Sci. Semicond. Process.* **16** 1619
27. Blanco M A *et al* 2004 *Comput. Phys. Commun.* **158** 57
28. Andersen O K 1975 *Phys. Rev. B* **42** 3063
29. Hohenberg P and Kohn W 1964 *Phys. Rev. B* **136** 864
30. Kohn W and Sham L J 1965 *Phys. Rev.* **140** 1133
31. Blaha P *et al* 2008 *WIEN2K, an augmented plane wave plus local orbitals program for calculating crystal properties* (Vienna, Austria)
32. Perdew J P *et al* 1996 *Phys. Rev. Lett.* **77** 3865
33. Wu Z and Cohen R E 2006 *Phys. Rev. B* **73** 235116
34. Perdew J P and Wang Y 1992 *Phys. Rev. B* **45** 13244
35. Engel E and Vosko S H 1993 *Phys. Rev. B* **47** 13164
36. Tran F and Blaha P 2009 *Phys. Rev. Lett.* **102** 226401
37. Becke A D and Johnson E R 2006 *J. Chem. Phys.* **124** 221101
38. Agrawal B K *et al* 1997 *J. Phys.: Condens. Matter* **9** 1763
39. Mohammad R and Katırcıoğlu S 2009 *J. Alloys Compd.* **469** 504
40. De Almeida J S and Ahuja R 2006 *Appl. Phys. Lett.* **89** 061913
41. Miloua R *et al* 2008 *Phys. Lett. A* **372** 1910
42. Murnaghan F D 1944 *Proc. Natl. Acad. Sci. USA* **30** 5390
43. Vegard L 1921 *Z. Phys.* **5** 17
44. Scharmann A *et al* 1979 *J. Lumin.* **18–19** 833
45. Ozawa L and Nagashima Y 1964 *J. Electrochem. Soc. Jpn.* **32** 26
46. Homann T *et al* 2006 *Solid State Sci.* **8** 44
47. Bernard J E and Zunger A 1986 *Phys. Rev. Lett.* **34** 5992
48. Swalin R A 1961 *Thermodynamics of solids* (New York: Wiley)
49. Ferreira L G *et al* 1999 *Phys. Rev. B* **40** 3197
50. Blanco M A *et al* 1996 *J. Mol. Struct. Theochem.* **368** 245
51. Flórez M *et al* 2002 *Phys. Rev. B* **66** 144112
52. Debye P 1912 *Ann. Phys.* **39** 789
53. Madelung O 1982 *Landolt Bornstein: numerical data and functional relationships in science and technology* vol. **17b**
54. Lee S G and Chang K J 1995 *Phys. Rev. B* **52** 1918
55. Hakan Gürel H *et al* 2012 *Superlattices Microstruct.* **51** 725
56. Hacini K *et al* 2011 *Comput. Mater. Sci.* **50** 3080
57. Khenata R *et al* 2006 *Comput. Mater. Sci.* **38** 29
58. Fleszar A and Hanke W 2005 *Phys. Rev. B* **71** 045207